Performance analysis of patch-type UHF-RFID tag antennas in the presence of mutual coupling

Fernand Konan Gbamele
Department of Electrical and Electronic Engineering, National Polytechnic Institute Félix HOUPHOUËT-BOIGNY (INP-HB) of Yamoussoukro, Ivory Coast.
Corresponding author: Fernand Konan GBAMELE (e-mail: kgbamel@ gmail.com).

ABSTRACT In a context of high-density deployment of UHF RFID patch-type tag antennas, mutual coupling can have an impact on the detection rate due to the degradation of the link budget between certain tags and the reader. The aim of this paper is to analyze the performance of a system that takes account of electromagnetic mutual coupling as a function of the random positions of UHF RFID patch-type tag antennas in complex environments. The design of the patch-types tags, including the extraction of the Y admittance parameters, was studied using the HFSS electromagnetic simulation software. To validate the study approach, the results obtained were compared using MATLAB software. The results obtained provide additional information needed to gain an in-depth understanding of UHF RFID patch-type tag antenna systems to make them reliable and practical in a dense environment. Future research and development work may be inspired in the design of UHF RFID patch-types tag antennas for miniaturized applications.

INDEX TERMS UHF RFID, patch-type tag, mutual coupling, coupling capacitance, admittance.

I. INTRODUCTION

Radio Frequency Identification (RFID) is a rapidly developing technology, and RFID sensors have become important components in many mainstream technology applications in recent years. With the rapid development of the logistics [1] and retail [2] industries, RFID technology is widely used in the logistics and retail industries. Radio Frequency Identification (RFID) is a non-contact automatic identification technology that uses radio frequency communication to perform functions such as tagging [3], managing safety on construction sites or other work scenarios [4], recording, storing and managing [5] the target object [6], identifying wagons arriving or departing from railway stations [7]. The most important component of the RFID system is the tag antenna structure. RFID antennas can be of the coil type, microstrip patch type, dipole type, inverted F antenna type or eight-wood type. With the development of logistics and retail, demand for RFID tag applications on metal surfaces is also increasing. However, these exceptional performances not only increase the price, but also increase the size and shorten the lifespan. Therefore, for effective use of RFID, it is crucial to understand the environment of use and the necessary conditions, which requires considerations in the deployment of patch-types of UHF RFID tag antennas. Coupling is critical where overlapping tags can introduce sufficiently large capacitance to have a significant impact on the intrinsic impedance of those tags in the UHF RFID band. The overlap area is also important for the introduction of reverse surface currents which are critical for the mismatched input impedance and its distorted radiation pattern and due to the high capacitance, the resonant frequency of the tag is reduced.

Some researchers have shown considerable interest in microstrip patch antennas for wearable devices due to their lightweight nature, simplicity of design, compact size, ease of manufacture, frequency tunability and compatibility with planar circuits [8]. An RFID microstrip patch antenna for tag identification on metal surfaces [9]. Another contribution in this context is a tag antenna designed to identify metal objects in the UHF band from 865 to 868 MHz [10]. Another miniaturized patch-type RFID tag antenna for mounting on metal surfaces has been proposed [11]. Another type of RFID patch tag antenna for applications involving metallic materials has been presented [12]. A planar UHF-RFID patch antenna for metallic applications has been proposed [13]. A folded microstrip patch antenna designed for passive RFID objects with metal foils has been proposed [14]. In view of the growing use of patch tags, a study is needed to investigate the impact of mutual coupling on RFID system performance when deployed in complex environments.

Most of the work does not address the problem of mutual coupling, which is one of the factors limiting the performance of UHF RFID. The patch-type tag antenna has a number of drawbacks, one of which is mutual coupling.

Mutual coupling results from a mutual influence between one of the patch antennas and the other, leading to a reduction in antenna performance such as gain, return loss, radiation profile, efficiency, channel capacity, corresponding impedance and transmitted power.

In an RFID context with a high density of patch-type tags, some studies have highlighted the impact of coupling. Mutual multi-patch type tag coupling has been studied [15] [16]. However, the tags are arranged on the same substrate. It is necessary to study the effect of mutual coupling in the reader zone, in a complex environment where several patch tags are deployed in UHF RFID applications.

The aim of this article is to analyze the degradation of the RFID communication link in a context of high patch-type tag antenna density. To our knowledge, the analysis based on additional coupling capacitances (C_{12} coupling in series and C_p equal frangible capacitances in shunt) has never been applied in an RFID link, in particular to assess the electromagnetic phenomenon of coupling. The study focuses mainly on the mutual coupling of two tag-type patch antennas placed in the near-field region of UHF RFID for different configurations and concentrated in a reduced volume. The near-patch region introduces additional capacitance and can be calculated using a pi network to extract the Z_{12} or Y_{12} or S_{12} parameters that model mutual coupling. For the two-element network, the electrical model is used to take into account the coupling between tag-type patch antennas. The additional coupling capacitances (C_{12} and C_p) are deduced from the value of Y_{12} at the resonant frequency for each distance.

The remainder of this manuscript is organized as follows. Section II deals with the design process of the UHF Patch-Type RFID tag antenna. The study of the effects of mutual coupling between several antennas is presented in Section III. Section IV presents the simulation results and comparisons. Finally, section V presents the conclusions.

II. DESIGN AND GEOMETRIC CONFIGURATION OF THE UHF RFID PATCH-TYPE TAG ANTENNA

A. ANTENNA GEOMETRY

The prototype UHF RFID patch tag used is a printed rectangular patch. The structure is designed to operate at the 868MHz frequency. The antenna geometry is shown in Fig. 1 and is mounted on a dielectric material with a thickness h=1.6mm. The dielectric used is FR4 epoxy resin with permittivity $\varepsilon_r = 4.4$. The antenna consists of a microstrip feed line and a rectangular radiating element into which notches have been inserted for impedance matching. Table I below gives the dimensions of the various components of the patch antenna.

TABLE I. Tag parameters

Parameters	Size (mm)
Patch width: W_p	102
Patch length : L_p	79.8
Notch length: L_N	30.5225
Notch width: W_N	3.191
Feed line width : L_f	35.8725
Feed line width: W_f	2.901

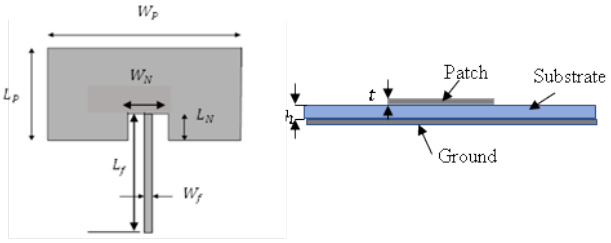

FIGURE 1. **Rectangular patch antenna with notches**

B. ANTENNA SIMULATION

The antenna design is modelled and simulated using software (HFSS High Frequency Simulation Structure), which can be used to study antenna performance (i.e. return loss, impedance, admittance and many other parameters). Fig. 2 shows the antenna geometry being excited by a discrete port assigned to the transmission feed line. The evolution of the reflection coefficient as a function of the excitation frequency is plotted in Fig. 3. The simulation results for the parameter of the optimized version of the antenna are in good agreement and show a good match at 868MHz. The antenna is well matched at 50Ω impedance (the normalized impedance around which most RF systems are designed) in the ISM band ($S_{11} \leq -11dB$).

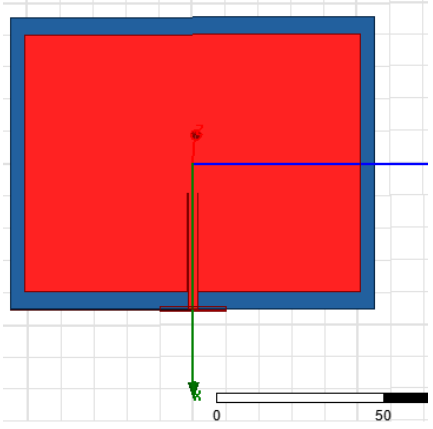

FIGURE 2. **Design of a patch antenna with notches under HFSS**

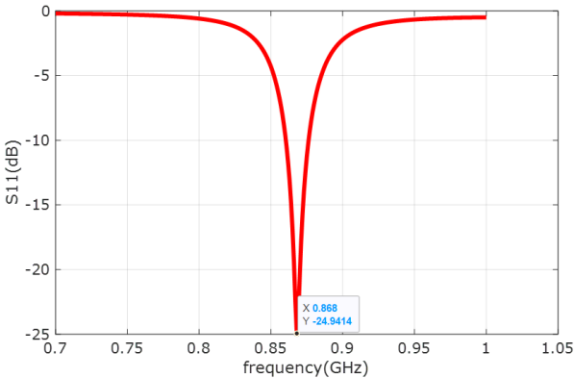

FIGURE 3. Reflection coefficient S_{11} of the patch-type tag antenna

C. ELECTRICAL CIRCUIT OF THE PATCH-TYPE TAG ANTENNA

Representing an antenna by an equivalent electrical circuit therefore saves time when studying the coupling between several tags in a package. The electrical model of the proposed tag antenna is shown in Fig.4.

The supply line is a lossless microstrip line. The electrical model of such a line is a parallel LC circuit [17] [18] [19]. The inductance and capacitance of the electrical model are denoted by L_f and C_f respectively in Fig.4

The characteristic admittance of the microstrip line can be given by equation (1):

$$Y_f = \frac{1}{j\omega L_f + \dfrac{1}{j\omega C_f + \dfrac{1}{j\omega L_f}}} \tag{1}$$

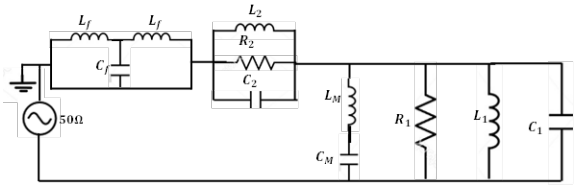

FIGURE 4. Electrical model of the proposed patch-type tag antenna

The printed rectangular microstrip patch is considered to be a combination, in parallel with a resistor R_1, of an inductance L_1 and a capacitance C_1. The admittance of the patch is given by equation (2) [18] [19]:

$$Y_p = \frac{1}{R_1} + j\left(\omega C_1 - \frac{1}{\omega L_1}\right) \tag{2}$$

When a notch is on the patch, the current distribution is modified in the radiating structure compared to the normal radiation of the patch. Consequently, this perturbation modifies the equivalent circuit of the initial patch by introducing an additional series inductance and a series capacitance. The final equivalent circuit of the notch is a parallel combination of a resistor R_2, inductance L_2 and capacitance C_2 is shown in Fig.4. The expressions for R_2, L_2 and C_2 are given in [18] [19]. The admittance of the notch is given by equation (3):

$$Y_2 = \frac{1}{R_2} + j\left(\omega C_2 - \frac{1}{\omega L_2}\right) \tag{3}$$

Note that the two resonant circuits, the rectangular patch and the loaded notch, are coupled by a mutual inductance L_M and a mutual capacitance C_M, and their expressions are given in [20] [21]. The admittance of the notch-patch coupling is calculated using equation (4):

$$Y_M = \frac{1}{j\omega L_M + \dfrac{1}{j\omega C_M}} \tag{4}$$

The equivalent circuit in admittance blocks is given in Fig.5. Therefore, the admittance of the patch-type tag antenna Y_1 of the printed rectangular patch system, feed line and notch can be calculated from Fig.5 is given by equation (5):

$$Y_1 = \frac{1}{\dfrac{1}{Y_f} + \dfrac{1}{Y_2} + \dfrac{1}{Y_f + Y_p}} \tag{5}$$

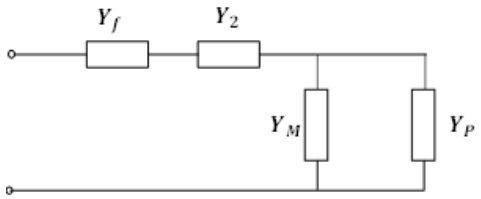

FIGURE 5. Equivalent circuit for the proposed patch-type tag antenna

To validate the equivalent circuit of the proposed patch, the Advanced Design System (ADS) circuit simulator based on the method of moments (MoM) was used. This is a commercial software package used for antenna design and development. The equivalent circuit of the patch antenna in the ADS platform is shown in Fig.6. The circuit parameters C_f, L_f, R_2, L_2, C_2, R_1, L_1, C_1, C_M and L_M are calculated using MATLAB software are grouped in Table II and then these values are imported into Advanced Design System (ADS) software the microwave and digital circuit simulator to fit the input impedance of $Z = 50\Omega$ as shown in Fig. 6.

TABLE II. Parametric value of the lumped equivalent circuit model

Lumped element	Value
Parch resistance: R_1	29.0369Ω
Parch inductance: L_1	0.14598nH
Parch capacity: C_1	230.25pF
Notch resistance: R_2	29.0369Ω
Notch inductance: L_2	0.48313nH
Notch capacity: C_2	230.25pF
Inductance of the feed line : L_f	0.6749nH
Feed line capacity : C_f	1.0369pF
Inductance of patch-notch coupling: L_M	0.4844nH
Patch-notch coupling capacity : C_M	0.06752pF

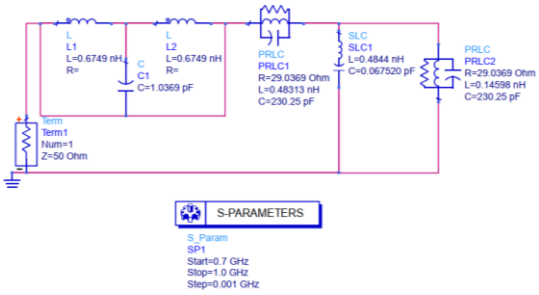

FIGURE 6. **Equivalent circuit for the UHF tag proposed under ADS.**

Fig.7 shows the comparison between the reflection loss of the antenna simulated in HFSS and the network model circuit simulated by ADS. Both curves resonate at exactly the same resonant frequency of 868MHz. The equivalent circuit is simulated and the values are compared with the simulation values from the simulation in Fig.3. The plots of the reflection coefficient, with $S_{11} = -11.538dB$ in the case of the ADS simulator and $S_{11} = -24.59414dB$ in the case of the HFSS simulator are shown in Fig.7.

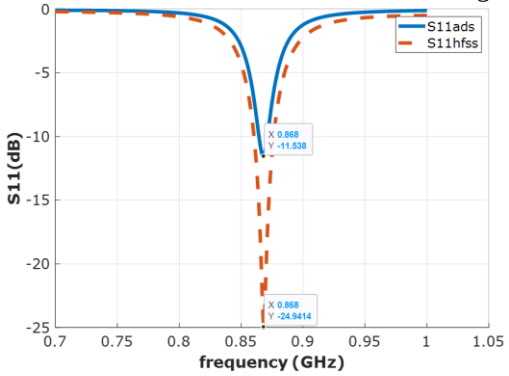

FIGURE 7. **Comparison of the reflection coefficient S_{11} of the tag under HFSS and ADS**

There is a good match at the same resonant frequency of 868 MHz, but the performance varies according to the software used. This is a very satisfactory result, since it shows that the equivalent circuit of the proposed notched patch antenna is valid. Good agreement was obtained between the two commercial software packages.

III. MODELLING THE MUTUAL COUPLING OF UHF RFID PATCH-TYPE TAG ANTENNAS IN HORIZONTAL AND VERTICAL CONFIGURATIONS

A. EQUIVALENT CIRCUIT FOR MUTUAL COUPLING

Consider two neighboring tags (tag1 and tag2) in a package of n identical tags. The two tags are simultaneously excited by the electromagnetic field of the RFID reader. The resultant total electromagnetic field is likely to be the sum of the elements radiated and the scattering fields from the two antennae. In a package the tags can be arranged randomly or in rows. The ratio s/λ between tags is assumed to be small (see Fig.8) (s, the distance between tag1 and tag 2, and λ, the wavelength). The RFID reader communicates with these tags in this configuration in order to retrieve the data they contain.

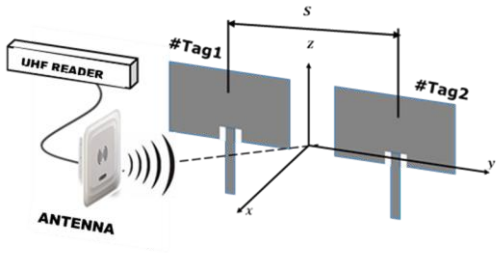

FIGURE 8. **Configuration of two coupled UHF RFID pach-type tag antennas**

The overlapping patches can introduce a sufficiently large capacitance which is crucial for lowering the resonant frequency in the useful UHF RFID band. The overlap area is also important for the introduction of reverse surface currents which are crucial for the generation of the polarisation insensitive radiation pattern and due to the high capacitance, the resonant frequency of the tag is reduced.

Whatever the configuration of the tags in the package, the equivalent circuit of two neighbouring tags is shown in Fig.9. Both tags are excited simultaneously by two discrete 50Ω ports (port #1: 50Ω and port #2: 50Ω). The system consists of the electrical models of tags 1 and 2, two frangible coupling capacitances C_{p_1}, C_{p_2} in shunt and a series coupling capacitance C_{12}. The coupling capacitances are highly dependent on the distance between the tags. The capacity C_{p_i} represents the parallel capacity of tag i due to the presence of tag j. The capacitance C_{ij} is the planar proximity serial capacitance of tags i and j. In the practical case, the radiating elements are supplied with currents of the same amplitude and phase, and the surface currents

created on each element are obtained from the matrix equation for two-port networks characterised by equation (6):

$$[I]=[Y].[V] \tag{6}$$

The following admittance matrix is extracted using equation (7) and given by equation (8):

$$\begin{cases} I_1 = Y_{11}V_1 + Y_{12}V_2 \\ I_2 = Y_{21}V_1 + Y_{22}V_2 \end{cases} \tag{7}$$

$$[Y]=\begin{bmatrix} Y_{11} & Y_{12} \\ Y_{21} & Y_{22} \end{bmatrix} \tag{8}$$

Fig.9 shows the equivalent electrical model of two identical printed antennas. The mutual coupling capacitance C_{12} of the π array obtained when the two patches are spaced s/λ. The Y-parameters of the pi (π) array are shown in Fig.10.

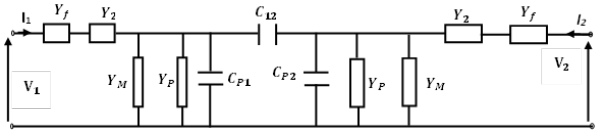

FIGURE 9. Proposed equivalent electrical circuit of two patch-type tag antennas

Fig.10 shows a simplified circuit of the elements shown in Fig.9.

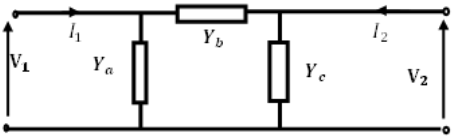

FIGURE 10. π - network of the two patch-type tag antennas

Y-parameters are also known as short-circuit admittance parameters. They are obtained as a ratio of current and voltage and the parameters are found by short-circuiting port 2 ($V_2 = 0$) or port 1 ($V_1 = 0$). Using equation (6) and equating the resulting circuit with a π -network, we obtain equations (9) and (10):

$$Y_{11} = Y_a + Y_b = Y_1 + j\omega\left(C_{p_1} + C_{12}\right) \tag{9}$$

$$Y_{12} = -Y_b = -j\omega C_{12} \tag{10}$$

The determination of the parasitic capacitances is based on the Y-parameters calculated from the combination of equations (9) and (10) and simulations using the HFSS software C_{12} and C_{p_1} are calculated from the Y-parameters calculated from this circuit with equations (1) and (12):

$$C_{12} = \left|-\mathrm{Im}(Y_{12})/\omega\right| \tag{11}$$

$$C_{p_1} = \left|\left(\mathrm{Im}(Y_{11}) - \mathrm{Im}\left(Y_1\right)\right)/\omega - C_{12}\right| \tag{12}$$

With

Y_1: self-admittance of the rectangular patch obtained from equation (5).

Since the two UHF-RFID patch-type tag antennas are identical for a two-port network, we can write $C_p = C_{p_1} = C_{p_2}$, $C_{12} = C_{21}$; $Y_{12} = Y_{21}$ et $Y_{22} = Y_{11}$ (reciprocity).

B. SIMULATIONS OF PATCH-TYPE TAG ANTENNAS IN THE HORIZONTAL CONFIGURATION

The different configurations of patch-type tag antennas modelled in HFSS are shown in the following figures. The simulation frequency is 868MHz. The distance between the tags varies by $0.4\lambda \le s \le 3\lambda$ while avoiding the tag edges. The coupling capacitance C_{12} is calculated using equation (11) for tag configurations arranged in the (Ox, Oy) plane. If one of the two antennas is excited, then both antennas are excited, so the resulting total electromagnetic field will be taken as the sum of the fields radiated and re-radiated by the two antenna elements.

Configuration 1: Patch-type tag antennas with parallel arrangement.

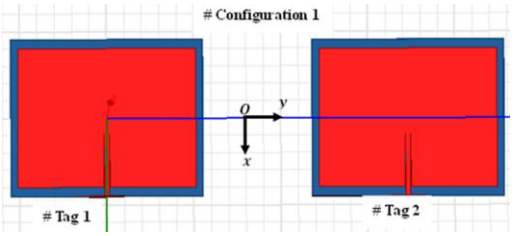

FIGURE 11. Simulation of an array of two patch-type tag antennas in a parallel arrangement.

Configuration 2: Patch-type tag antennas with opposing feeds.

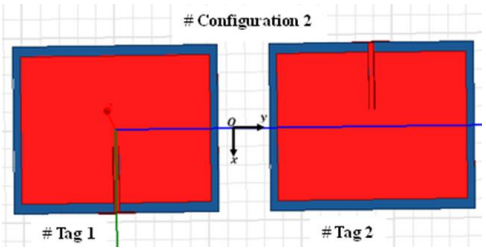

FIGURE 12. Simulation of the network of two patch-type tag antennas with opposite feeds.

Configuration 3: Patch-type tag antennas with opposite side feeds.

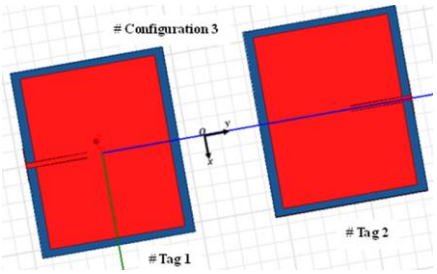

FIGURE 13. Simulation of an array of two patch-type tag antennas with opposite side feeds.

Configuration 4: Patch-type tag antennas with orthogonal arrangement.

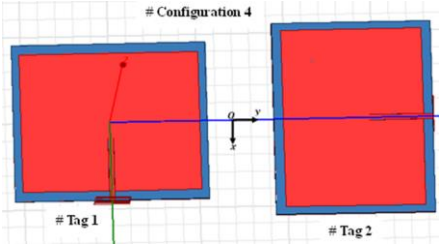

FIGURE 14. Simulation of an array of two patch-type tag antennas with orthogonal arrangement.

Configuration 5: Patch-type tag antennas with the same side feeds.

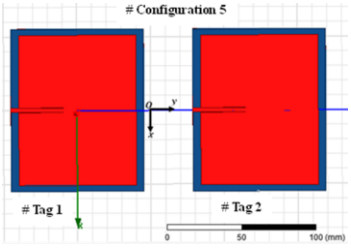

FIGURE 15. Simulation of an array of two patch-type tag antennas with the same side feeds.

Configuration 6 : Patch-type tag antennas, one of which is placed in the (Ox,Oz) plane.

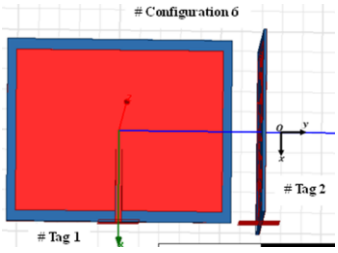

FIGURE 16 Simulation of an array of two patch-type tag antennas, one of which is placed in the (Ox, Oz) plane.

Configuration 7 : Patch-type tag antennas with tag 2 inclined at an angle $\theta = 45^{\circ}$ to the axis (Oz).

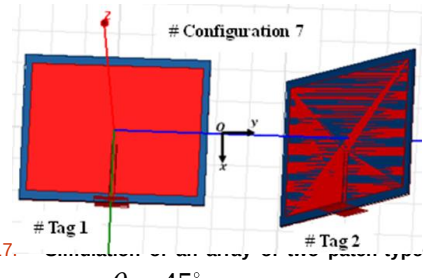

FIGURE 17. **Simulation of an array of two patch-type tag antennas, with tag 2 inclined by $\theta = 45^{\circ}$ with respect to the axis (Oz).**

C. SIMULATIONS OF PATCH-TYPE TAG ANTENNAS IN THE VERTICAL CONFIGURATION

As before, the distance between tags varies between $0.2\lambda \le s \le 3\lambda$ while also avoiding tag edges. The coupling capacitance C_{12} for some configurations of the arrangements where the tag centres are aligned along the (Oz) axis. The different antenna configurations modelled using HFSS are shown in the following figures. The simulation frequency is 868MHz. The coupling capacitance C_{12} for two configurations of the arrangements along the axis (Oz) of the tags.

Configuration 1: Patch-type tag antennas arranged along the (Oz) axis (collinear).

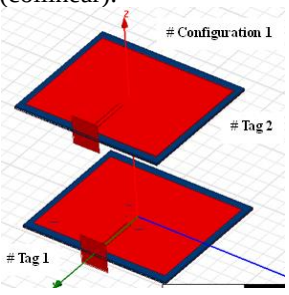

FIGURE 18. Simulation of an array of two patch-type tag antennas arranged along the (Oz) axis (collinear).

Configuration 2 : Patch-type tag antennas with tag 2 tilted by $\theta = 45^{\circ}$ with respect to the axis (Oz).

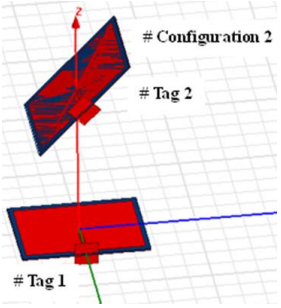

FIGURE 19. **Simulation of an array of two patch-type tag antennas with tag 2 tilted by $\theta = 45^{\circ}$ with respect to the axis (Oz).**

Configuration 3 : Tag-type patch antennas with tag 2 parallel to the axis (Oz) and perpendicular to tag 1.

FIGURE 20. **Simulation of an array of two tag-type patch antennas with tag 2 parallel to the axis (Oz) and perpendicular to tag 1.**

Configuration 4: Patch-type tag antennas with face-to-face arrangement.

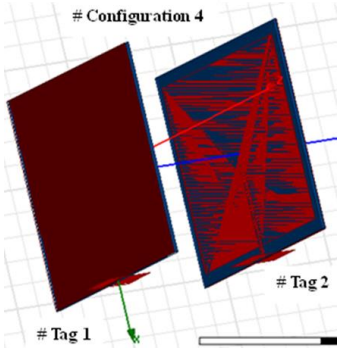

FIGURE 21. **Simulation of an array of two patch-type tag antennas in a face-to-face arrangement.**

IV. RESULTS AND DISCUSSION

A. C_{12} COUPLING CAPACITY IN HORIZONTAL AND VERTICAL CONFIGURATIONS

The simulation results for these configurations are shown in Fig.22.

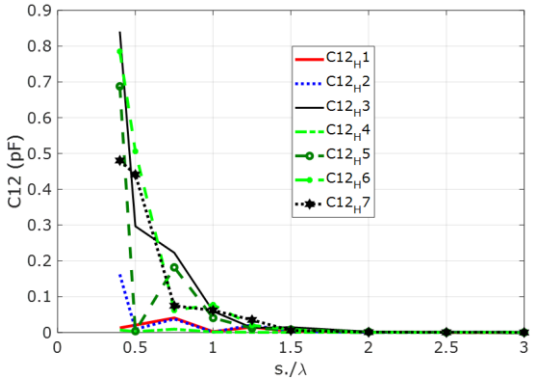

FIGURE 22. **Comparison of C_{12} coupling capacities for horizontal configurations.**

Fig. 22 shows comparisons of the C_{12} capacitance as a function of the ratio s/λ. It can be seen that the coupling capacitance C_{12} depends strongly on the distance between the UHF RFID patch-type tag antennas. The #4 orthogonal configuration shows a high level of isolation compared with the other configurations. The #4 orthogonal configuration shows a high level of isolation compared with the other configurations. This mutual coupling capability is due to the polarization where the E-field vectors have a perpendicular orientation, which inherently minimizes the coupling energy between the elements and increases their isolation. Parallel configuration #1 also shows a high level of isolation but not like configuration #4. This configuration is also recommended for parallel arrangements of UHF RFID patch-type tag antennas in complex environments. Configurations #2, #3, #5, #6 and #7 have high C_{12} coupling capacitances compared with configurations #1 and #4. In general, it can be seen that as the distance increases, the C_{12} capacitance between the two patches tends towards zero, causing the mutual effect of far-field coupling to gradually decrease towards zero. It should be noted here that the coupling capacitance cancels out above $s \succ 0.5\lambda$ for certain configurations.

The simulation results for these configurations are shown in Fig.23.

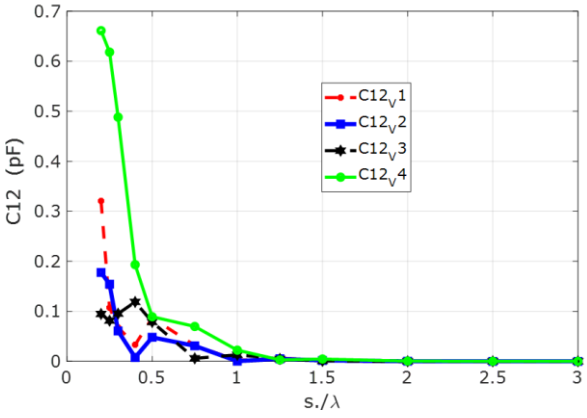

FIGURE 23. **Comparison of C_{12} coupling capacities for vertical configurations.**

The simulation results of the four configurations show that the coupling capacity C_{12} is high for all four configurations for distances $s \leq 0.5\lambda$ and on the other hand, if the distance $s \succ 0.5\lambda$ between the tags is very large, the coupling capacity C_{12} gradually decreases to zero. The simulation result for configuration #4 in which the two tags are opposite each other is the highest and higher than configurations #1, #2 and #3 for $s \leq 0.5\lambda$.

Configurations #1, #2 and #3 coupling capacitance are almost the same. It should be noted here that the coupling capacitance C_{12} cancels out below $s \succ 0.5\lambda$. It should also be noted that the coupling capacitance cancels out below $s \succ \lambda$ for all configurations and remains high for $s \prec \lambda$.

A. COUPLING CAPACITY C_p IN HORIZONTAL AND VERTICAL ONFIGURATIONS

The parallel coupling capacitance of the network $C_p = C_{p_1} = C_{p_2}$ obtained when the two patches are spaced by s/λ. The HFSS software can be used to calculate the natural admittance Y_{11}. The value of Y_1 is calculated using equation (12). The resonant frequency gives us the coupling capacitances C_p. he results are shown in Figs. 24 and 25, using Matlab software. In Fig.25, the capacitance $C_{pj}V$ with $j \in \{1,2,3,4\}$ (parallel coupling capacitance for displacement along the Oz axis) for the different configurations and in Fig.25, the capacitance $C_{p_i}H$ with $i \in \{1,2,3,4,5,6,7\}$ (parallel coupling capacitance for displacement along the Oy axis).

Fig.24, the parallel coupling capacitance $C_{p_i}H$ for the different s/λ ratios between the two UHF RFID patch-type tag antennas. The results show that for configurations #2, #3, #4, #5 and #7, when $s \prec 0.5\lambda$ a weak trend in coupling capacity $C_{p_i}H$ is observed, while for configurations #1 and #6 it tends to increase. This shows that these configurations are not recommended for large-scale deployment of UHF RFID patch-type tag antennas since the coupling is high.

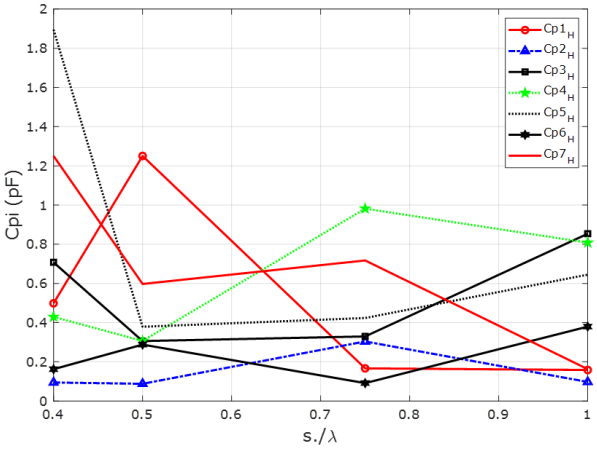

FIGURE 24. **Comparison of coupling capacities $C_{p_i}H$ for horizontal configurations.**

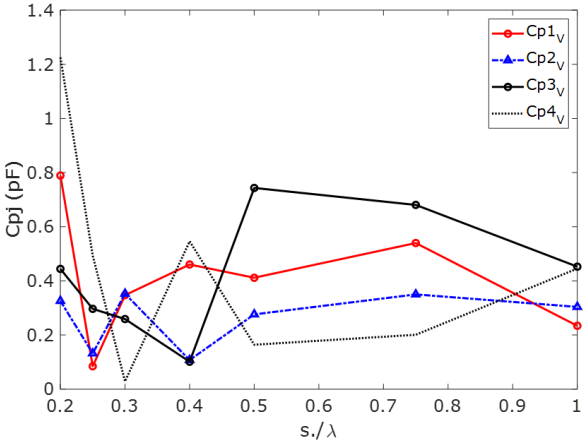

FIGURE 25. **Comparison of coupling capacities $C_{pj}V$ for vertical configurations.**

Fig.25 shows the results obtained from the pararel coupling capacitance $C_{pj}V$ for a displacement along the Oz axis. Smaller differences are observed between calculated coupling capacities $C_{pj}V$. It can also be seen that the calculated coupling capacities vary less for small values of distance $s \prec 0.5\lambda$. The same trends are observed as in the case where $s \succ 0.5\lambda$.

V. CONCLUSION

This article presents a rapid method for obtaining the mutual coupling of UHF RFID patch-type tag antennas and describes the parallel coupling capacity ignored in most studies. The coupling capacitance values obtained show that it is important to take into account the phenomenon of mutual coupling between UHF RFID patch-type tags in their design and deployment. The results are consistent with the literature and open up prospects for evaluating the coupling of several tag stacks whose antenna are not necessarily patch-type tag antenna.

REFERENCES

[1] X. Cao, L. Tiffany, and Q. Wang, “RFID-based multi-attribute logistics information processing and anomaly mining in production logistics”,vol.57,no.17,pp.5453-5466,2019. https://doi.org/10.1080/00207543.2018.1526421

[2] M. Škiljo, Z. Blažević and T. Perković, “Analysis of passive RFID applicability in a retail store: What can we expect?”, *Sensors*, pp. 2038,vol.20,no.7,pp.2038,2020. https://doi.org/10.3390/s20072038,

[3] H. Kamaludin, H. Mahdin and J. H. Abawajy, “Clone tag detection in distributed RFID systems”, *PloS one*, vol. 13, no 3, p. e0193951, 2018. https://doi.org/10.1371/journal.pone.0193951

[4] T. Montanaro, I. Sergi, A. Motroni, A. Buffi, P. Nepa, M. Pirozzi, L. Catarinucci, R. Colella, F.P. Chietera, L. Patrono., “An IoT-aware smart system exploiting the electromagnetic behavior of UHF-RFID tags to improve worker safety in outdoor environments”, *Electronics*,vol.11,no.5,pp.717,2022. https://doi.org/10.3390/electronics11050717

[5] X. Han and H. Li, “Design of Food Logistics Vehicle Management System Based on RFID Technology”, *Packaging and Food Machinery / Pack Food Mach*, Vol. 39, no. 3, pp. 73-77, 2021. https://doi.org/10.3969/j.issn.1005-1295.2021.03.013

[6] B. Pawłowicz, B. Trybus, M. Salach and P. Jankowski-Mihułowicz, "Dynamic RFID identification in urban traffic management systems", *Sensors*, vol. 20, no.15, pp. 4225, 2020. https://doi.org/10.3390/s20154225

[7] X. Zhang and T. Manos, "Applications of fast-moving RFID tags in high-speed railway systems", *International journal of engineering business management*, vol.3, pp.6 ,2011. https://doi.org/10.5772/45676

[8] M. Sharma, "Design and analysis of multiband antenna for wireless communication », *Wireless Personal Communications*, 114, no.2, pp.1389-1402, 2020. https://doi.org/10.1007/s11277-020-07425-9

[9] S. Zhang, Y. Gong and G. Zhu, "Detection Method Based on RFID Tag on the Metal Surface", *Journal of Physics: Conference Series*,Vol.2395,no.1,pp.012037,2022. https://doi.org/10.1088/1742-6596/2395/1/012037

[10] Q. Z. Chen and B. J. Hu, "Novel UHF RFID tag antenna with shorted stubs mountable on the metallic objects", *International Conference on Microwave and Millimeter Wave Technology*, Vol. 4,pp.1822-1824,2008. https://doi.org/10.1109/ICMMT.2008.4540834

[11] S.L. Chen, "A miniature RFID tag antenna design for metallic objects application", *IEEE Antennas and Wireless Propagation Letters*,vol.8,pp.1043-1045,2009. https://doi.org/10.1109/LAWP.2009.2032252

[12] S. L. Chen, K. H. Lin and R. Mittra, "A low profile RFID tag designed for metallic objects", *Asia Pacific Microwave Conference*,pp.226-228,2009. https://doi.org/10.1109/APMC.2009.5385320

[13] M. S. R. Bashri, M. I. Ibrahimy and S. M. A. Motakabber, "A planar wideband inductively coupled feed patch antenna for UHF RFID tag", *IEEE International Conference on RFID-Technologies andApplications(RFID-TA)*,pp.1-6,2013. https://doi.org/10.1109/RFID-TA.2013.6694504

[14] W. H. Ng, E. H. Lin and B. K. Chung, "Compact folded patch antenna for UHF RFID", *Progress in Electromagnetics Research Symposium - Fall (PIERS - FALL)*, pp. 132-134, 2017. https://doi.org/10.1109/PIERS-FALL.2017.8293125

[15] P. Wang; L. Dong, H. Wang; G. Li; Y. Di; X. Xie; D. Huang, "Passive Wireless Dual-Tag UHF RFID Sensor System for Surface Crack Monitoring", *Sensors*,vol.21,no3,pp.882,2021. https://doi.org/10.3390/s21030882

[16] P. Wang; L. Dong, H. Wang; G. Li; Y. Di; X. Xie; D. Huang, "Investigation the influence of miniaturized RFID tag sensor on coupling effect", *Sensor Review*, Vol. 41 No. 4, pp. 425-435, 2021. https://doi.org/10.1108/SR-04-2021-0138

[17] M.K. Meshram and B.R. Vishvakarma, "Gap coupled microstrip array antenna for wide band operation", *International Journal of Electronics*,pp.1161-1175,2001. https://doi.org/10.1080/00207210110071288

[18] M. Meada, "Analysis of gap in microstrip Transmission Line", *IEEE Trans. Antennas and Propagation*, pp. 1375-1379, 1972.

[19] R. Garg, P. Bhartia, I. Bahl and A. Ittipiboon, "Microstrip Antenna Design Handbook", Norwood, MA, Boston (USA), pp.253-263, 2001.

[20] V. K. Pandey and B. R. Vishvakarma, "Theoretical analysis of linear array antenna of stacked patches", *Indian Journal of Radio and Space Physics*, pp. 125-130, 2005.

[21] X.X. Zheng, and F. Yang, "Study of slit cut microstrip antenna and its application", Microwave Optical Technology. Lett, vol. 18, no 4, pp. 297-300., 1998. https://doi.org/10.1002/(SICI)1098-2760(199807)18:4<297: AID-MOP14>3.0.CO;2-1